

RESEARCH ARTICLE | MAY 03 2024

Size-dependent photoluminescence blinking mechanisms and volume scaling of biexciton Auger recombination in single CsPbI₃ perovskite quantum dots

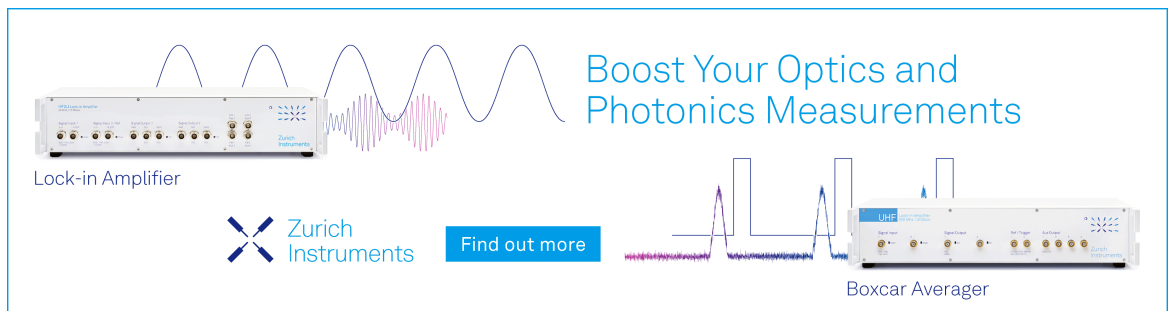
Special Collection: [Light-matter Interaction at the Nano and Molecular Scale](#)

Changgang Yang ; Guofeng Zhang ✉; Yunan Gao ; Bin Li ; Xue Han ; Jialu Li ; Mi Zhang ; Zihao Chen ; Yixin Wei; Ruiyun Chen ; Chengbing Qin ; Jianyong Hu ; Zhichun Yang ; Ganying Zeng ; Liantuan Xiao ✉; Suotang Jia




J. Chem. Phys. 160, 174505 (2024)

<https://doi.org/10.1063/5.0199389>



Boost Your Optics and Photonics Measurements

Lock-in Amplifier

 Zurich Instruments

[Find out more](#)

Boxcar Averager

Size-dependent photoluminescence blinking mechanisms and volume scaling of biexciton Auger recombination in single CsPbI₃ perovskite quantum dots

Cite as: J. Chem. Phys. 160, 174505 (2024); doi: 10.1063/5.0199389

Submitted: 22 January 2024 • Accepted: 18 April 2024 •

Published Online: 3 May 2024



View Online



Export Citation



CrossMark

Changgang Yang,^{1,2} Guofeng Zhang,^{1,2,a)} Yunan Gao,^{2,3} Bin Li,^{1,2} Xue Han,^{1,2} Jialu Li,^{1,2} Mi Zhang,^{1,2} Zhihao Chen,^{1,2} Yixin Wei,^{1,2} Ruiyun Chen,^{1,2} Chengbing Qin,^{1,2} Jianyong Hu,^{1,2} Zhichun Yang,^{1,2} Ganying Zeng,^{1,2} Liantuan Xiao,^{1,2,a)} and Suotang Jia^{1,2}

AFFILIATIONS

¹State Key Laboratory of Quantum Optics and Quantum Optics Devices, Institute of Laser Spectroscopy, Shanxi University, Taiyuan, Shanxi 030006, China

²Collaborative Innovation Center of Extreme Optics, Shanxi University, Taiyuan, Shanxi 030006, China

³State Key Laboratory for Mesoscopic Physics and Frontiers Science Center for Nano-optoelectronics, School of Physics, Peking University, Beijing 100871, China

Note: This paper is part of the JCP Special Topic on Light-matter Interaction at the Nano and Molecular Scale.

a) Authors to whom correspondence should be addressed: guofeng.zhang@sxu.edu.cn and xlt@sxu.edu.cn

ABSTRACT

Determining the correlation between the size of a single quantum dot (QD) and its photoluminescence (PL) properties is a challenging task. In the study, we determine the size of each QD by measuring its absorption cross section, which allows for accurate investigation of size-dependent PL blinking mechanisms and volume scaling of the biexciton Auger recombination at the single-particle level. A significant correlation between the blinking mechanism and QD size is observed under low excitation conditions. When the QD size is smaller than their Bohr diameter, single CsPbI₃ perovskite QDs tend to exhibit BC-blinking, whereas they tend to exhibit Auger-blinking when the QD size exceeds their Bohr diameter. In addition, by extracting bright-state photons from the PL intensity trajectories, the effects of QD charging and surface defects on the biexcitons are effectively reduced. This allows for a more accurate measurement of the volume scaling of biexciton Auger recombination in weakly confined CsPbI₃ perovskite QDs at the single-dot level, revealing a superlinear volume scaling ($\tau_{XX,Auger} \propto \sigma^{1.96}$).

Published under an exclusive license by AIP Publishing. <https://doi.org/10.1063/5.0199389>

I. INTRODUCTION

Inexpensive and straightforward colloidal techniques can be used to efficiently obtain high-quality all-inorganic CsPbX₃ perovskite quantum dots (QDs).¹ The CsPbX₃ perovskite QDs may contain Cl⁻, Br⁻, I⁻, or mixed halide systems Cl⁻/Br⁻ and Br⁻/I⁻. They possess valuable optical properties, such as bright photoluminescence (PL), tunable bandgaps that cover the entire visible spectrum, and excellent PL quantum yields (QYs).²⁻⁴ The CsPbX₃ perovskite QDs have great potential for use in optoelectronic applications. Previous studies have shown that CsPbX₃ perovskite QDs can be used for low-threshold lasing and highly effective

light-emitting devices.^{5,6} These QDs also have potential for use in quantum light sources, which could be important for future quantum communication and precision measurements.^{7,8} The size of perovskite QDs is a crucial factor affecting their PL properties and applications.^{9,10} The characterization of QD size is typically achieved through electron microscopy, while the PL properties of single QDs are measured using optical methods based on confocal microscopy. However, correlating the size of the same QD with its PL properties in two different experimental setups presents a significant challenge.

PL blinking is a phenomenon commonly observed in colloidal QDs during single-QD investigations.¹¹⁻¹⁶ It refers to the irregular

switching of PL intensity between bright (on) and dim (off) states while under constant excitation, which affects the QD emission and associated applications. Previous studies have identified two main blinking mechanisms for colloidal QDs: Auger-blinking and band-edge carrier (BC)-blinking.^{17–23} Due to the neutralization and photoionization of QDs, Auger-blinking trajectories exhibit distinct bright and dim states. The charging model of Auger-blinking suggests that the bright and dim states result from the radiative recombination of neutral exciton and charged (trion) states, respectively.^{12,13,24} Although the radiative rate of the trion state is twice that of the neutral exciton state, the nonradiative Auger recombination of the trion state effectively quenches PL. Auger-blinking requires long-lived traps capable of capturing photoexcited carriers for long periods of time until a second exciton is produced to form the trion state.^{13,25} Auger-blinking with different radiative and nonradiative rates results in a nonlinear correlation between PL lifetime and intensity.^{13,18} BC-blinking differs from Auger-blinking in that it exhibits various emission states with different nonradiative rates, while its radiative rate remains constant.^{26,27} According to the multiple recombination centers (MRCs) model of BC-blinking, various emission states originate from the activation and deactivation of a set of nonradiative recombination centers.²⁷ These nonradiative recombination centers are short-lived traps for band-edge carriers. When BC-blinking occurs with varying nonradiative rates and a fixed radiative rate, a linear correlation between PL lifetime and intensity is observed.

Based on the two blinking mechanisms mentioned above, PL blinking is primarily caused by the trapping and de-trapping of carriers by the short- or long-lived traps. Both short-lived and long-lived traps in perovskite QDs are believed to arise from the surface defects. The short-lived traps have faster trapping and de-trapping rates, while the long-lived traps have slower trapping and de-trapping rates. The trapping and de-trapping rates are determined by the degree of overlap between the wave functions of the excitons and the surface defects.²⁸ The size of the QDs directly affects this overlap, which in turn has a critical impact on PL blinking. The blinking behaviors of various perovskite (MAPbBr₃, FAPbBr₃, CsPbBr₃, and CsPbI₃) QDs of different sizes have been investigated, including strongly (QD size is smaller than their Bohr diameter), moderately (close to their Bohr diameter), and weakly (larger than their Bohr diameter) confined QDs in the size range of 2–20 nm.^{8,9,20–22,26,29–32} However, it is worth noting that both BC- and Auger-blinking have been observed in perovskite QDs with weak to intermediate quantum confinement,^{21,22,29,30} as well as in those with strong quantum confinement.^{8,26,31} It should be noted that colloidal QD samples typically have a wide size distribution. In addition, higher excitation conditions result in the occurrence of Auger-blinking.^{22,26,28} To determine if there is a correlation between the size of a QD and its blinking mechanism, correlation measurements must be taken under low excitation conditions.

Nonradiative Auger recombination not only causes Auger-blinking but also dominates multiexciton recombination.^{33,34} The Auger recombination rate of multiexciton is known to decrease as the volume of QDs increases.³⁵ This is due to two reasons. First, the Auger effect is mediated by reduced carrier–carrier Coulomb interactions in larger-volume QDs. Second, there is a tightening of the momentum conservation requirements that becomes apparent

at larger sizes. An accurate investigation of the volume scaling of biexciton Auger recombination (the correlation between the Auger recombination rate of biexciton and QD volume) is important for both fundamental physics and applications, as multiexciton effects exhibit a nonlinear dependence on the number of excitons and are usually dominated by biexciton contributions. Previous studies have investigated the volume scaling of biexciton Auger recombination for CsPbBr₃, CsPbI₃, and MAPbBr₃ perovskite QDs.^{9,36–42} It has been found that perovskite QDs exhibit varying volume scaling under different quantum confinements. For strong confinement, the biexciton lifetime shows a linear dependence on the perovskite QD volume ($\tau_{XX,Auger} \propto V^{1.0}$),^{36,38,42} which is similar to the dependence observed for conventional Cd- and Pb-based QDs.^{43,44} In the weak confinement regime, the dependence becomes sublinear as the perovskite QD size increases beyond the Bohr diameter ($\tau_{XX,Auger} \propto V^{0.38-0.5}$).^{9,36,38,39} This sublinear volume scaling has been attributed to a bimolecular Auger interaction.⁴⁵ The interaction is a two-body process where each exciton is formed in a different part of the nanomaterial. However, Huang *et al.* reported a superlinear volume scaling of biexciton Auger recombination lifetime for large CsPbBr₃ nanocrystals [$\tau_{XX,Auger} \propto V^\alpha$ ($\alpha > 1$)] and provided an interpretation using a nonlocal interaction model.^{40,41} Studies on ensembles of weakly confined perovskite QDs have given inconsistent results, suggesting the need to investigate their volume scaling at the single-QD level.

In this study, we investigate the size-dependent blinking mechanisms and volume scaling of biexciton Auger recombination in single CsPbI₃ perovskite QDs. While it is not feasible to measure the size of a single QD using optical methods, its absorption cross section can be measured by single-QD spectroscopy. The absorption cross section is directly proportional to the QD volume, $\sigma \propto V$,^{38,46} and can, therefore, be used to represent the QD size. The fluorescence lifetime intensity distribution (FLID) maps and the ratio of radiative rates were analyzed to determine the PL blinking mechanisms of single CsPbI₃ perovskite QDs of different sizes. A significant correlation between the blinking mechanism and QD size was observed for the first time under low excitation conditions. Furthermore, we obtained the volume scaling of biexciton Auger lifetimes of single CsPbI₃ perovskite QDs with weak confinement by measuring their biexciton lifetimes and QYs. Our results show a superlinear increase in Auger recombination lifetime with QD volume, i.e., $\tau_{XX,Auger} \propto V^{1.96}$.

II. RESULTS AND DISCUSSION

To investigate the size-dependent PL blinking mechanisms and volume scaling of biexciton Auger recombination for single perovskite QDs, we synthesized a high-quality sample of CsPbI₃ perovskite QDs with a wide size distribution using the hot injection method by appropriately slowing down the injection rate of the Cs-precursor solution (refer to the supplementary material for details). The PL spectrum of the CsPbI₃ perovskite QDs is centered at 655 nm with a full width at the half maximum of 46 nm, as shown in Fig. 1(a). The PL QY of the QD sample exceeds 85%. The transmission electron microscopy (TEM) image of the QDs is displayed in the inset of Fig. 1(b). The histogram of QD sizes indicates a size distribution ranging from 6 to 16 nm [Fig. 1(b)].

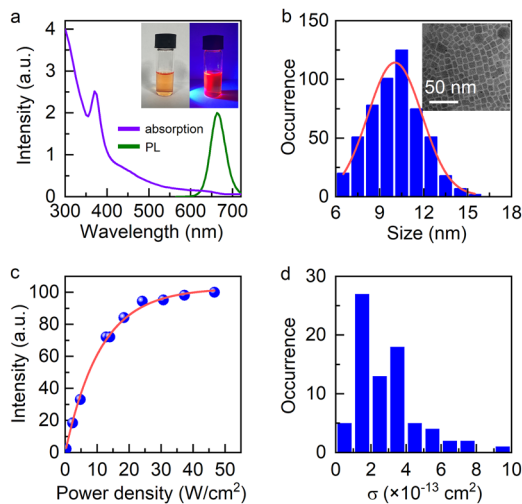


FIG. 1. (a) Absorption and photoluminescence (PL) spectra of CsPbI₃ perovskite quantum dots (QDs) dispersed in hexane. Inset: photographs of the resulting solution under room temperature and UV light. (b) Size histogram of CsPbI₃ perovskite QDs. Inset: transmission electron microscopy (TEM) image. (c) Typical PL saturation curve for a single CsPbI₃ perovskite QD. (d) Histogram of the absorption cross sections of CsPbI₃ perovskite QDs.

The size of single QDs can be represented by their absorption cross section since the absorption cross section is proportional to the QD volume.^{38,46} By recording the PL intensity of a single QD at different excitation powers (Fig. S1), the PL saturation curve of the single QD can be obtained. The absorption cross section (σ) can then be determined by fitting the PL saturation curve with the equation $I \propto 1 - e^{-\sigma j}$,^{25,46,47} where j represents the excitation photon flux. The excitation photon flux can be calculated using $j = P/FE$, where P is the laser power density, F is the laser repetition rate, and E is the laser photon energy. To improve the accuracy of the absorption cross section, the contribution of multi-exciton photons to the saturation curve is eliminated.⁴⁸ Figure 1(c) displays a typical PL saturation curve for single CsPbI₃ perovskite QDs, which is fitted to determine the absorption cross section of $1.60 \times 10^{-13} \text{ cm}^2$. Approximately 80 CsPbI₃ perovskite QDs of varying sizes were analyzed for their absorption cross section values. The histogram of absorption cross section values is presented in Fig. 1(d), indicating a wide distribution.

The size-dependent blinking mechanisms of single CsPbI₃ perovskite QDs are first investigated. Time-tagged, time-resolved, and time-correlated single-photon counting (TTTR-TCSPC) is used to record photon arrival times and laser synchronized pulses for each QD. The resulting data are used to construct PL intensity traces, decay curves, second-order correlation function curves [$g^{(2)}(\tau)$], and FLID maps for single QDs. Subsequently, the saturation curve of each QD is measured to determine its absorption cross section. Typical PL blinking trajectories for a relatively small-sized CsPbI₃ perovskite QD and a relatively large-sized CsPbI₃ perovskite QD are shown in Figs. 2(a) and 2(b), respectively. The values of absorption cross section for the two QDs were determined to be 1.61×10^{-13} and $5.11 \times 10^{-13} \text{ cm}^2$, respectively. To eliminate the impact of excitation power on PL blinking, we used a low excitation condition (N) of

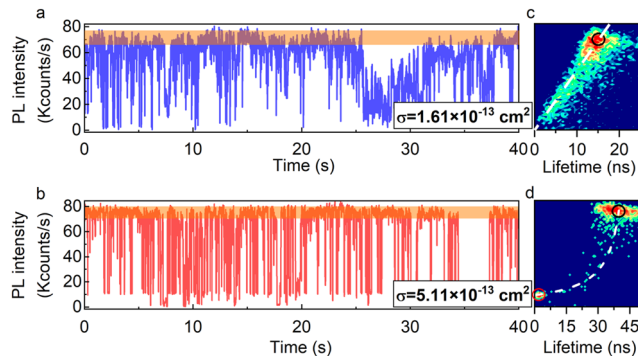


FIG. 2. (a) and (b) Typical PL blinking trajectories of a relatively small-sized CsPbI₃ perovskite single QD ($\sigma = 1.61 \times 10^{-13} \text{ cm}^2$) and a relatively large-sized CsPbI₃ perovskite single QD ($\sigma = 5.11 \times 10^{-13} \text{ cm}^2$). (c) and (d) Corresponding fluorescence intensity-lifetime distribution (FLID) maps. The white dotted lines in the FLID maps are the simulated lines using Eqs. (1) and (2), respectively. The linear FLID map indicates the BC-blinking, and the nonlinear FLID map indicates the Auger-blinking.

~ 0.1 for measuring all QDs. Here, $\langle N \rangle$ represents the average number of photons absorbed per QD per pulse and can be determined by $\langle N \rangle = j\sigma$.^{26,48} The PL blinking trajectory of the small-sized CsPbI₃ perovskite QD displays fluctuations between a series of continuously distributed emission states. On the other hand, the PL blinking trajectory of the large-sized CsPbI₃ perovskite QD can be approximated as “binary blinking,”⁴⁹ where the PL intensity alternates between a bright state and a dim state.

Figures 2(c) and 2(d) present the corresponding FLID maps, which can effectively identify blinking mechanisms.^{12,13} The lifetime values in the FLID maps are obtained by averaging the arrival time of each bin’s PL photons.^{12,18} The FLID map of the small-sized CsPbI₃ perovskite QD exhibits an approximately linear correlation between PL intensity (I) and lifetime (τ) [Fig. 2(c)]. This correlation can be accurately simulated by Eq. (1),¹³ as shown by the white dotted line in Fig. 2(c),

$$I \propto QY = \frac{k_r}{k_r + k_{nr}(t)} = \tau k_r = \frac{\tau}{\tau_r}, \quad (1)$$

where QY and k_r represent the PL QY and radiation recombination rate of single CsPbI₃ perovskite QDs, respectively. The good simulation indicates that the blinking mechanism of the QD is BC-blinking.

Compared to the FLID map of the small-sized CsPbI₃ perovskite QD, the FLID map of the large-sized CsPbI₃ perovskite QD exhibits a non-linear distribution [see Fig. 2(d)]. The FLID map displays dim and bright states with PL intensities of 10.3 Kcounts/s (I_2 , red cycle) and 75.1 Kcounts/s (I_1 , black cycle), respectively. The corresponding lifetime values are 2.7 ns (τ_2) and 39.7 ns (τ_1), respectively. Therefore, the ratio of radiative rates between the dim and bright states ($\beta = I_2\tau_1/I_1\tau_2$) is ~ 2 , indicating that the dim and bright states correspond to the trion and single exciton states, respectively.^{13,15} This is because the trion state has two recombination channels for two electrons (holes) and one hole (electron), so its radiative rate is twice that of the single exciton state.⁵⁰ The presence of the trion state may imply that the observed PL blinking

in Fig. 2(b) is Auger-blinking. The FLID map of Auger-blinking can be simulated using Eq. (2),^{13,18} as shown by the white dotted line in Fig. 2(d),

$$I = \frac{I_1 I_2 (\tau_2 - \tau_1)}{I_2 (\tau_2 - \tau) + I_1 (-\tau_1 + \tau)}. \quad (2)$$

The good simulation indicates that Eq. (2) can effectively reproduce the curved FLID map, suggesting that the observed PL blinking in the large-sized CsPbI₃ perovskite QD is Auger-blinking.

To investigate the size-dependent blinking mechanisms in single CsPbI₃ perovskite QDs, we analyzed the PL blinking mechanisms of ~80 QDs with absorption cross section ranging from 0.5×10^{-13} to 9.3×10^{-13} cm², and the histograms are shown in Fig. 3(a). The blue and red histograms correspond to BC-blinking and Auger-blinking, respectively. The histograms show that single CsPbI₃ perovskite QDs exhibit mainly BC-blinking when their absorption cross section is smaller than 2×10^{-13} cm², and Auger-blinking when the absorption cross section is larger than 3×10^{-13} cm². We speculate that the Bohr diameter of CsPbI₃ perovskite QDs may be a critical value for both blinking mechanisms. Thus, the absorption cross section value for CsPbI₃ perovskite QDs with the size of their Bohr diameter (12 nm³⁴⁻³⁷) should fall within the range of 2×10^{-13} to 3×10^{-13} cm². To verify this, we investigate the correlation between the absorption cross section and the peak of the emission spectra of the single CsPbI₃ perovskite QDs. Previous research has shown that the peak of the PL spectrum of CsPbI₃ perovskite QDs with a size close to the Bohr diameter is located at 680 nm.⁵¹ Therefore, the absorption cross section value corresponding to the CsPbI₃ perovskite QDs with the size of a Bohr diameter can be inferred from the correlation between the absorption cross section and the peak of the emission spectra.

Figure 3(b) shows two typical PL spectra of single CsPbI₃ perovskite QDs with absorption cross section values of 1.30×10^{-13} and 6.85×10^{-13} cm², respectively. The peak position of each QD's PL emission spectrum was obtained through Lorentz fitting. The absorption cross section values of 1.30×10^{-13} and 6.85×10^{-13} cm² correspond to PL spectral peaks at 673 and 685 nm, respectively. We obtained the PL spectral peak positions of single CsPbI₃ perovskite

QDs as a function of absorption cross sections by measuring ~40 QDs, as shown in Fig. 3(c). The distribution of PL spectral peak positions can be fitted using a power function ($y \propto \sigma^{-2}$), as indicated by the red curve in Fig. 3(c). Based on the fitting result, the single CsPbI₃ perovskite QDs with the PL emission peak of 680 nm correspond to an absorption cross section value of 2.60×10^{-13} cm². This suggests that the absorption cross section value of CsPbI₃ perovskite QD with the size of its Bohr diameter is $\sim 2.60 \times 10^{-13}$ cm². The absorption cross section value of 2.60×10^{-13} cm², corresponding to the Bohr diameter of CsPbI₃ perovskite QDs, falls within the range of 2×10^{-13} and 3×10^{-13} cm², as indicated by the dotted line in Fig. 3(a). This suggests that the Bohr diameter is the critical value for both blinking mechanisms, as expected. The reason for this correlation should be easy to comprehend. Perovskite QDs do not have a shell layer, and their size can directly affect the capture of carriers by the surface defects.²⁸ Small-sized perovskite QDs, with a size smaller than the Bohr diameter of their bulk material, have excitons with wave functions that significantly overlap with those of the surface defects, leading to fast trapping and de-trapping of carriers. As a result, the surface defects behave as short-lived traps, and PL blinking exhibits BC-blinking. Perovskite QDs larger than the Bohr diameter have exciton wave functions with less overlap with those of the surface defects. This leads to slower trapping and de-trapping of carriers. As a result, the surface states behave as long-lived traps, and PL blinking exhibits Auger-blinking. Therefore, the size of the QDs determines the overlap of wave functions between excitons and the surface states, which is correlated with the blinking mechanisms.

Here, we analyze the possible reasons why such a clear correlation between QD size and the blinking mechanism has not been observed in previous studies. One possible explanation is that previous studies did not measure the correlation between the blinking behavior of each QD and its size. Instead, they used the average size to express the QD size, whereas the QD samples typically have a wide size distribution. When the size distribution of a QD sample covers its Bohr diameter, both BC blinking and Auger blinking were observed in the same QD sample, resulting in an insignificant correlation between the QD size and the blinking mechanism. Furthermore, higher excitation conditions may result in the occurrence of Auger blinking in small-sized QDs. Recent research has shown

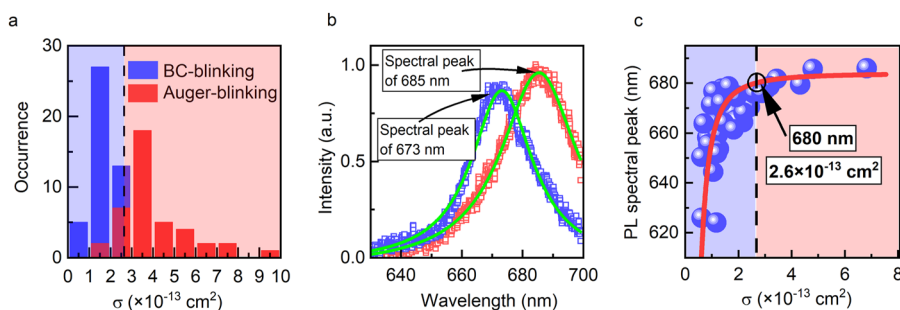


FIG. 3. (a) Histograms of size-dependent blinking mechanisms for single CsPbI₃ perovskite QDs. The size of the QDs is represented by the absorption cross section. Single QDs mainly exhibit BC-blinking when the absorption cross section of single QDs is smaller than 2×10^{-13} cm², and Auger-blinking when the absorption cross section is larger than 3×10^{-13} cm². (b) Typical PL spectra of single CsPbI₃ perovskite QDs with absorption cross section values of 1.30×10^{-13} cm² (blue) and 6.85×10^{-13} cm² (red), respectively. The green curves represent Lorentz's fits. (c) PL spectral peak positions of single CsPbI₃ perovskite QDs as a function of absorption cross sections and fitted with the function $\propto \sigma^{-2}$.

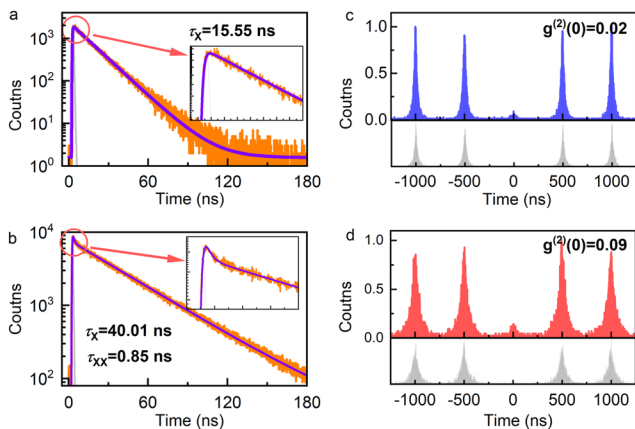


FIG. 4. (a) and (b) Typical PL decay curves for the small- and large-sized CsPbI₃ perovskite QDs extracted from the bright state PL regions marked in the PL intensity trajectories of Figs. 2(a) and 2(b). The PL decay curves of the small- and large-sized CsPbI₃ perovskite QDs can be fitted by a single exponential and a biexponential function, respectively, as shown by the purple solid lines. The insets are zoomed-in views. The solid gray lines are the instrument response function of the system. (c) and (d) Corresponding second-order correlation function [$g^{(2)}(\tau)$] curves for the small- and large-sized CsPbI₃ perovskite QDs, respectively. The gray curves on the lower panels are the time-gated $g^{(2)}(\tau)$ curves.

that the blinking type in small-sized QDs changes from BC blinking to Auger blinking as the laser fluence increases.²⁸ This suggests that both small- and large-sized QDs exhibit Auger blinking under higher excitation conditions, which weakens the correlation between QD size and the blinking mechanism. In addition, poor preparation of QD samples also results in BC blinking in large-sized QDs. All these factors may contribute to a weak correlation between QD size and the blinking mechanism.

In addition to the PL blinking, we investigated the volume scaling of biexciton Auger recombination of perovskite QDs with different sizes by analyzing their PL decay curves and $g^{(2)}(\tau)$ curves. Figures 4(a) and 4(b) show the PL decay curves extracted from the bright-state PL regions marked in the PL intensity trajectories of Figs. 2(a) and 2(b). The extraction of the bright-state PL regions can effectively reduce the effects of charged and trap states on the biexcitons, thus enabling more accurate biexciton information to be obtained.⁵² The PL decay curve of the small-sized CsPbI₃ perovskite QD can be fitted by a single exponential function, indicating that these bright-state photons are almost exclusively due to single exciton emission.⁵³ In contrast, the PL decay curve of the large-sized CsPbI₃ perovskite QD exhibits an extremely fast decay component (0.85 ns), as shown in the inset of Fig. 4(b). The fast decay component in the bright-state is attributed to the recombination of biexcitons, similar to the case of the well-studied CdSe/CdS and CdSe/ZnS core/shell QDs.^{48,49,53} The comparison of the PL decay curves of the small- and large-sized CsPbI₃ perovskite QDs indicates more biexciton emission in the latter. Large-sized QDs can effectively reduce the carrier-carrier Coulomb interactions and, thus, attenuate the nonradiative Auger recombination.^{10,33,35,39} Therefore, relatively strong biexciton emission can be observed in the large-sized CsPbI₃ perovskite QDs.

Furthermore, we investigate the effect of size on the biexciton QY using the $g^{(2)}(\tau)$ method.⁵⁴ Under weak excitation ($\langle N \rangle < 0.3$), the biexciton QY of a single QD is approximately equal to the $g^{(2)}(0)$ value.⁵⁴ The $g^{(2)}(0)$ value can be determined from the ratio of the central peak area and the side peak area of the $g^{(2)}(\tau)$ curve. The $g^{(2)}(\tau)$ curves of bright-state PL regions for the small- and large-sized CsPbI₃ perovskite QDs are shown in Figs. 4(c) and 4(d), respectively. The $g^{(2)}(0)$ value of 0.09 for the large-sized CsPbI₃ perovskite QD is significantly larger than that of the small-sized CsPbI₃ perovskite QD (0.02), indicating that large-sized perovskite QDs have a higher biexciton QY. Note that the $g^{(2)}(0)$ values here are more accurately obtained by subtracting the $g^{(2)}(0)$ values of the time-gated $g^{(2)}(\tau)$ curves [gray curves in Figs. 4(c) and 4(d)] from the $g^{(2)}(0)$ values of the original $g^{(2)}(\tau)$ curves, eliminating the contribution of background photons in $g^{(2)}(0)$ values [for the method of constructing the time-gated $g^{(2)}(\tau)$ curves, see the previous work^{22,55}]. The biexciton QYs of about 70 single CsPbI₃ perovskite QDs of different sizes were obtained by this method. The biexciton QYs of single CsPbI₃ perovskite QD as a function of absorption cross sections are shown in Fig. 5(a). The biexciton QY of single CsPbI₃ perovskite QDs increases almost linearly from 0.01 to 0.18 as the absorption cross section increases from 0.56×10^{-13} to 9.34×10^{-13} cm², which is consistent with the recent report for single CsPbBr₃ perovskite

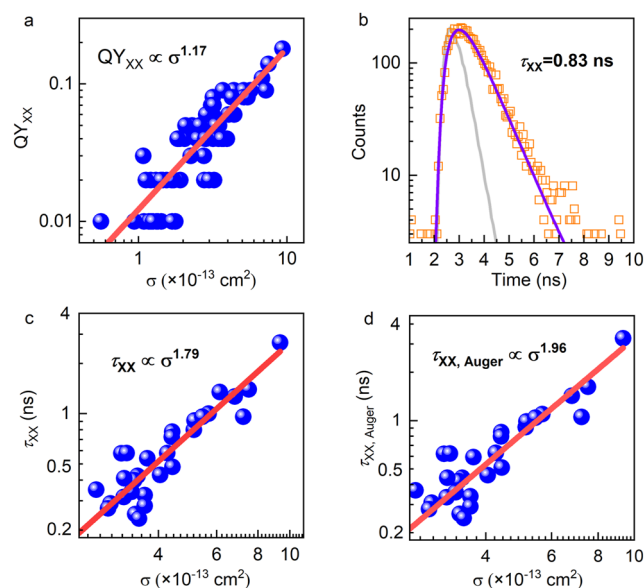


FIG. 5. (a) Biexciton QYs as a function of absorption cross sections for single CsPbI₃ perovskite QDs. (b) Typical PL decay curve of biexciton for single large-sized CsPbI₃ perovskite QDs. The purple solid line represents the single exponential function fit. The gray solid line is the system instrument response function. (c) Biexciton lifetimes as a function of absorption cross sections for weakly confined CsPbI₃ perovskite QDs ($\sigma > 2.6 \times 10^{-13}$ cm²). (d) Biexciton Auger lifetimes as a function of absorption cross sections for weakly confined CsPbI₃ perovskite QDs. The biexciton Auger lifetime exhibits a dependence on absorption cross section that can be described by superlinear volume scaling $\tau_{XX,Auger} \propto V^{1.96}$.

QDs.⁵⁶ It is worth noting that the biexciton QY of single CsPbI₃ perovskite QDs is smaller than that of single CsPbBr₃ perovskite QDs. This is due to the fact that the Bohr diameter of CsPbI₃ (12 nm) is larger than that of CsPbBr₃ (7 nm).¹⁰ At the same particle size, the CsPbI₃ QDs have stronger confinement, resulting in a smaller biexciton QY. In addition, from the PL decay and $g^{(2)}(\tau)$ curves, we can see that the small-sized CsPbI₃ perovskite QDs have very few biexciton photons, and it is difficult to obtain their biexciton lifetimes. Therefore, we only investigate the biexciton Auger recombination in the weakly confined CsPbI₃ perovskite QDs ($\sigma > 2.6 \times 10^{-13} \text{ cm}^2$).

For CsPbI₃ perovskite QDs with weak confinement, the biexciton decay curves of bright-states in their PL trajectories can be obtained using first-photon analysis. Figure 5(b) shows a typical biexciton decay curve extracted from the bright-state PL region of the PL intensity trajectory in Fig. 2(b). The biexciton lifetime of 0.83 ns was determined by fitting the decay curve with a single exponential function, which closely matches the result obtained from the biexponential function fitting in Fig. 4(b). The biexciton lifetimes of ~28 weakly confined CsPbI₃ perovskite QDs (with $\sigma > 2.6 \times 10^{-13} \text{ cm}^2$) were obtained by using first-photon analysis. Figure 5(c) shows the biexciton lifetimes as a function of absorption cross sections, which exhibit a superlinear characteristic. By combining the biexciton QY and the lifetime of each QD, it is possible to calculate the biexciton Auger lifetime using the following equation:

$$\tau_{XX,A} = \frac{\tau_{XX}}{1 - QY_{XX}}, \quad (3)$$

where τ_{XX} and QY_{XX} are the biexciton lifetime and QY, respectively.

The biexciton Auger lifetimes of ~28 single CsPbI₃ perovskite QDs as a function of absorption cross sections are shown in Fig. 5(d), which was fitted to obtain the volume scaling of the biexciton Auger lifetime ($\tau_{XX,Auger} \propto \sigma^{1.96}$). The absorption cross section σ is proportional to the QD volume V , thus $\tau_{XX,Auger} \propto V^{1.96}$. The results are consistent with Huang *et al.*'s recent report that the biexciton Auger lifetime in weakly confined perovskite nanocrystals increases superlinearly with volume,⁴⁰ which is attributed to nonlocal effects.^{40,41} It is worth noting that both our results and those of Huang *et al.* deviate from the sublinear results found in earlier research.^{9,36,38} Here, we briefly analyze the possible causes of the deviations. Compared to the sublinear volume scaling, the superlinear volume scaling implies longer biexciton Auger lifetimes, and hence longer biexciton lifetimes and larger biexciton QYs [see Eq. (3)]. We note that early studies were conducted at the ensemble level, and the ensemble measurements do not easily eliminate the effects of QD charging and surface defects on biexcitons. QD charging and surface defects can introduce nonradiative recombination, thereby reducing biexciton lifetimes and QYs.^{22,25} Therefore, the biexciton Auger lifetimes previously measured for QD ensembles may be smaller. However, in our single-QD study, we extracted biexciton lifetimes and QYs from the bright states in PL intensity trajectories. This approach effectively reduces the effects of QD charging and surface defects on the biexciton lifetimes and QYs, resulting in longer biexciton Auger lifetimes. Furthermore, Huang *et al.* used high-quality, large perovskite nanocrystals in their study.⁴⁰ The PL intensity trajectories of these nanocrystals showed minimal blinking behavior, indicating a low presence of QD charging and surface defects. Therefore, longer biexciton Auger lifetimes were observed, resulting in superlinear volume

scaling. In addition, different dielectric environments, such as liquid or solid interfaces, where the QDs are located can also affect the biexciton lifetimes.^{48,57}

Here, we use the ratio of the radiative lifetimes of single excitons to those of biexcitons to verify the accuracy of the biexciton Auger lifetimes obtained above. As the single exciton QY in the bright state of the PL intensity trajectory is typically considered to be unity,⁵² the radiative lifetime of a single exciton is equal to the single exciton lifetime. According to the biexciton lifetimes and QYs shown in Figs. 5(a) and 5(c), the biexciton radiative lifetimes can be calculated by $\tau_{XX,r} = \tau_{XX}/QY_{XX}$. The average ratio of the single exciton radiative lifetime to the biexciton radiative lifetime for single CsPbI₃ perovskite QDs is calculated to be 4.3 ± 0.8 , which is close to the theoretical value of 4.^{25,58,59} This indicates that the obtained biexciton Auger lifetimes are accurate.

III. CONCLUSION

The size-dependent blinking mechanisms and volume scaling of biexciton Auger recombination in CsPbI₃ perovskite QDs have been investigated using single QD spectroscopy. Correlated measurements of the size of the same QD and its PL properties are achieved by measuring the QD absorption cross section to determine the size. The results showed a clear correlation between QD size and blinking mechanism under low excitation conditions. When the size of CsPbI₃ perovskite QDs is smaller than their Bohr diameter, they tend to exhibit BC-blinking. Conversely, if the size exceeds their Bohr diameter, they tend to exhibit Auger-blinking. In addition, by extracting the bright-state photons from the PL intensity trajectories, the biexciton lifetimes and QYs have been accurately measured. The volume scaling of biexciton Auger recombination of weakly confined CsPbI₃ perovskite QDs at the single-dot level was obtained, revealing a superlinear characteristic. Determining the size-dependent properties of perovskite QDs can provide valuable guidance for selecting the optimal particle size in various perovskite QD applications, ultimately enhancing their overall performance.

SUPPLEMENTARY MATERIAL

The supplementary material file contains typical PL intensity trajectories at different excitation powers, CsPbI₃ perovskite QD synthesis, single QD sample preparation, and experimental setups.

ACKNOWLEDGMENTS

The authors acknowledge the financial support from the National Key Research and Development Program of China (No. 2022YFA1404201), the Natural Science Foundation of China (Nos. 62127817, U22A2091, U23A20380, 62075120, 62222509, 62075122, 62205187, 62105193, 62305201, and 62305200), NSFC-STINT (No. 62011530133), Program for Changjiang Scholars and Innovative Research Team (No. IRT_17R70), China Postdoctoral Science Foundation (No. 2022M722006), Fundamental Research Program of Shanxi Province (Nos. 202303021222031, 202103021223032, and 202103021223254), Shanxi Province Science and Technology Innovation Talent Team (No. 202204051001014), Shanxi Province Science and Technology Major Special Project (No. 202201010101005),

Science and Technology Cooperation Project of Shanxi Province (No. 202104041101021), Shanxi “1331 Project,” and 111 Project (No. D18001).

AUTHOR DECLARATIONS

Conflict of Interest

The authors have no conflicts to disclose.

Author Contributions

All authors commented on the manuscript. The manuscript was prepared with the contributions of all authors. All authors agree to the final version of the manuscript.

Changgang Yang: Conceptualization (equal); Data curation (equal); Formal analysis (equal); Funding acquisition (equal); Investigation (lead); Methodology (lead); Project administration (lead); Resources (lead); Supervision (lead); Validation (lead); Writing – original draft (lead); Writing – review & editing (lead). **Guofeng Zhang:** Conceptualization (lead); Data curation (lead); Formal analysis (lead); Funding acquisition (lead); Investigation (lead); Methodology (lead); Project administration (lead); Resources (lead); Supervision (lead); Validation (lead); Writing – original draft (lead); Writing – review & editing (lead). **Yunan Gao:** Writing – original draft (equal); Writing – review & editing (equal). **Bin Li:** Data curation (equal); Funding acquisition (supporting); Software (lead); Writing – original draft (equal); Writing – review & editing (equal). **Xue Han:** Data curation (equal); Methodology (equal); Writing – original draft (equal); Writing – review & editing (equal). **Jialu Li:** Data curation (equal); Methodology (equal); Software (equal); Writing – original draft (supporting); Writing – review & editing (supporting). **Mi Zhang:** Data curation (supporting); Methodology (supporting). **Zhihao Chen:** Data curation (supporting); Writing – original draft (supporting). **Yixin Wei:** Data curation (supporting); Software (supporting). **Ruiyun Chen:** Funding acquisition (equal); Writing – original draft (equal); Writing – review & editing (equal). **Chengbing Qin:** Funding acquisition (equal); Writing – original draft (equal); Writing – review & editing (equal). **Jianyong Hu:** Funding acquisition (equal); Writing – original draft (equal); Writing – review & editing (equal). **Zhichun Yang:** Funding acquisition (equal); Writing – original draft (equal); Writing – review & editing (equal). **Ganying Zeng:** Funding acquisition (equal); Writing – original draft (equal); Writing – review & editing (equal). **Liantuan Xiao:** Conceptualization (lead); Data curation (lead); Formal analysis (lead); Funding acquisition (lead); Investigation (lead); Methodology (lead); Project administration (lead); Resources (lead); Supervision (lead); Validation (lead); Writing – original draft (lead); Writing – review & editing (lead). **Suotang Jia:** Funding acquisition (lead); Writing – original draft (equal); Writing – review & editing (equal).

DATA AVAILABILITY

The data that support the findings of this study are available from the corresponding authors upon reasonable request.

REFERENCES

- 1 L. Protesescu, S. Yakunin, M. I. Bodnarchuk, F. Krieg, R. Caputo, C. H. Hendon, R. X. Yang, A. Walsh, and M. V. Kovalenko, “Nanocrystals of cesium lead halide perovskites (CsPbX_3 , X = Cl, Br, and I): Novel optoelectronic materials showing bright emission with wide color gamut,” *Nano Lett.* **15**(6), 3692–3696 (2015).
- 2 A. Dutta, R. K. Behera, P. Pal, S. Baitalik, and N. Pradhan, “Near-unity photoluminescence quantum efficiency for all CsPbX_3 (X=Cl, Br, and I) perovskite nanocrystals: A generic synthesis approach,” *Angew. Chem., Int. Ed.* **58**(17), 5552–5556 (2019).
- 3 S. Sun, D. Yuan, Y. Xu, A. Wang, and Z. Deng, “Ligand-mediated synthesis of shape-controlled cesium lead halide perovskite nanocrystals via reprecipitation process at room temperature,” *ACS Nano* **10**(3), 3648–3657 (2016).
- 4 H. Huang, L. Polavarapu, J. A. Sichert, A. S. Susha, A. S. Urban, and A. L. Rogach, “Colloidal lead halide perovskite nanocrystals: Synthesis, optical properties and applications,” *NPG Asia Mater.* **8**(11), e328 (2016).
- 5 X. Li, Y. Wu, S. Zhang, B. Cai, Y. Gu, J. Song, and H. Zeng, “ CsPbX_3 quantum dots for lighting and displays: Room-temperature synthesis, photoluminescence superiorities, underlying origins and white light-emitting diodes,” *Adv. Funct. Mater.* **26**(15), 2435–2445 (2016).
- 6 B. Tang, H. Dong, L. Sun, W. Zheng, Q. Wang, F. Sun, X. Jiang, A. Pan, and L. Zhang, “Single-mode lasers based on cesium lead halide perovskite submicron spheres,” *ACS Nano* **11**(11), 10681–10688 (2017).
- 7 H. Utzat, W. Sun, A. E. K. Kaplan, F. Krieg, M. Ginterseder, B. Spokoyny, N. D. Klein, K. E. Shulenberger, C. F. Perkinson, M. V. Kovalenko, and M. G. Bawendi, “Coherent single-photon emission from colloidal lead halide perovskite quantum dots,” *Science* **363**(6431), 1068–1072 (2019).
- 8 Y. S. Park, S. Guo, N. S. Makarov, and V. I. Klimov, “Room temperature single-photon emission from individual perovskite quantum dots,” *ACS Nano* **9**(10), 10386–10393 (2015).
- 9 T. Kim, S. I. Jung, S. Ham, H. Chung, and D. Kim, “Elucidation of photoluminescence blinking mechanism and multiexciton dynamics in hybrid organic-inorganic perovskite quantum dots,” *Small* **15**(33), 1900355 (2019).
- 10 C. Zhu, M. Marczak, L. Feld, S. C. Boehme, C. Bernasconi, A. Moskalenko, I. Cherniukh, D. Dirin, M. I. Bodnarchuk, M. V. Kovalenko, and G. Rainò, “Room-temperature, highly pure single-photon sources from all-inorganic lead halide perovskite quantum dots,” *Nano Lett.* **22**(9), 3751–3760 (2022).
- 11 J. Shi, W. Sun, H. Utzat, A. Farahvash, F. Y. Gao, Z. Zhang, U. Barotov, A. P. Willard, K. A. Nelson, and M. G. Bawendi, “All-optical fluorescence blinking control in quantum dots with ultrafast mid-infrared pulses,” *Nat. Nanotechnol.* **16**(12), 1355–1361 (2021).
- 12 C. Galland, Y. Ghosh, A. Steinbruck, M. Sykora, J. A. Hollingsworth, V. I. Klimov, and H. Htoon, “Two types of luminescence blinking revealed by spectroelectrochemistry of single quantum dots,” *Nature* **479**(7372), 203–207 (2011).
- 13 G. C. Yuan, D. E. Gomez, N. Kirkwood, K. Boldt, and P. Mulvaney, “Two mechanisms determine quantum dot blinking,” *ACS Nano* **12**(4), 3397–3405 (2018).
- 14 C. G. Yang, G. F. Zhang, L. H. Feng, B. Li, Z. J. Li, R. Y. Chen, C. B. Qin, Y. Gao, L. T. Xiao, and S. T. Jia, “Suppressing the photobleaching and photoluminescence intermittency of single near-infrared CdSeTe/ZnS quantum dots with p-phenylenediamine,” *Opt. Express* **26**(9), 11889–11902 (2018).
- 15 C. G. Yang, R. L. Xiao, S. R. Zhou, Y. G. Yang, G. F. Zhang, B. Li, W. L. Guo, X. Han, D. H. Wang, X. Q. Bai, J. L. Li, R. Y. Chen, C. B. Qin, J. Y. Hu, L. H. Feng, L. T. Xiao, and S. T. Jia, “Efficient, stable, and photoluminescence intermittency-free CdSe-based quantum dots in the full-color range,” *ACS Photonics* **8**(8), 2538–2547 (2021).
- 16 J. L. Li, D. F. Wang, G. F. Zhang, C. G. Yang, W. L. Guo, X. Han, X. Q. Bai, R. Y. Chen, C. B. Qin, J. Y. Hu, L. T. Xiao, and S. T. Jia, “The role of surface charges in the blinking mechanisms and quantum-confined Stark effect of single colloidal quantum dots,” *Nano Res.* **15**(8), 7655–7661 (2022).
- 17 H. Yoshimura, M. Yamauchi, and S. Masuo, “In situ observation of emission behavior during anion-exchange reaction of a cesium lead halide perovskite nanocrystal at the single-nanocrystal level,” *J. Phys. Chem. Lett.* **11**(2), 530–535 (2020).

- ¹⁸C. T. Trinh, D. N. Minh, K. J. Ahn, Y. Kang, and K. G. Lee, "Verification of Type-A and Type-B-HC blinking mechanisms of organic-inorganic formamidinium lead halide perovskite quantum dots by field measurements," *Sci. Rep.* **10**(1), 2172 (2020).
- ¹⁹S. Mandal, S. Mukherjee, C. K. De, D. Roy, S. Ghosh, and P. K. Mandal, "Extent of shallow/deep trap states beyond the conduction band minimum in defect-tolerant CsPbBr₃ perovskite quantum dot: Control over the degree of charge carrier recombination," *J. Phys. Chem. Lett.* **11**(5), 1702–1707 (2020).
- ²⁰T. Ahmed, S. Seth, and A. Samanta, "Mechanistic investigation of the defect activity contributing to the photoluminescence blinking of CsPbBr₃ perovskite nanocrystals," *ACS Nano* **13**(11), 13537–13544 (2019).
- ²¹S. Seth, T. Ahmed, and A. Samanta, "Photoluminescence flickering and blinking of single CsPbBr₃ perovskite nanocrystals: Revealing explicit carrier recombination dynamics," *J. Phys. Chem. Lett.* **9**(24), 7007–7014 (2018).
- ²²B. Li, H. Huang, G. F. Zhang, C. G. Yang, W. L. Guo, R. Y. Chen, C. B. Qin, Y. Gao, V. P. Biju, A. L. Rogach, L. T. Xiao, and S. T. Jia, "Excitons and biexciton dynamics in single CsPbBr₃ perovskite quantum dots," *J. Phys. Chem. Lett.* **9**(24), 6934–6940 (2018).
- ²³X. Bai, H. Li, Y. Peng, G. Zhang, C. Yang, W. Guo, X. Han, J. Li, R. Chen, C. Qin, J. Hu, G. Yang, H. Zhong, L. Xiao, and S. Jia, "Role of aspect ratio in the photoluminescence of single CdSe/CdS dot-in-rods," *J. Phys. Chem. C* **126**(5), 2699–2707 (2022).
- ²⁴M. Nirmal, B. O. Dabbousi, M. G. Bawendi, J. J. Macklin, J. K. Trautman, T. D. Harris, and L. E. Brus, "Fluorescence intermittency in single cadmium selenide nanocrystals," *Nature* **383**(6603), 802–804 (1996).
- ²⁵B. Li, G. Zhang, Y. Zhang, C. Yang, W. Guo, Y. Peng, R. Chen, C. Qin, Y. Gao, J. Hu, R. Wu, J. Ma, H. Zhong, Y. Zheng, L. Xiao, and S. Jia, "Biexciton dynamics in single colloidal CdSe quantum dots," *J. Phys. Chem. Lett.* **11**, 10425–10432 (2020).
- ²⁶X. Han, G. F. Zhang, B. Li, C. G. Yang, W. L. Guo, X. Q. Bai, P. Huang, R. Y. Chen, C. B. Qin, J. Y. Hu, Y. F. Ma, H. Z. Zhong, L. T. Xiao, and S. T. Jia, "Blinking mechanisms and intrinsic quantum-confined Stark effect in single methylammonium lead bromide perovskite quantum dots," *Small* **16**(51), 2005435 (2020).
- ²⁷P. A. Frantsuzov, S. Volkan-Kacso, and B. Janko, "Model of fluorescence intermittency of single colloidal semiconductor quantum dots using multiple recombination centers," *Phys. Rev. Lett.* **103**(20), 207402 (2009).
- ²⁸C. Yang, Y. Li, X. Hou, M. Zhang, G. Zhang, B. Li, W. Guo, X. Han, X. Bai, J. Li, R. Chen, C. Qin, J. Hu, L. Xiao, and S. Jia, "Conversion of photoluminescence blinking types in single colloidal quantum dots," *Small* (published online, 2023).
- ²⁹N. Yarita, H. Tahara, M. Saruyama, T. Kawawaki, R. Sato, T. Teranishi, and Y. Kanemitsu, "Impact of postsynthetic surface modification on photoluminescence intermittency in formamidinium lead bromide perovskite nanocrystals," *J. Phys. Chem. Lett.* **8**(24), 6041–6047 (2017).
- ³⁰C. T. Trinh, D. N. Minh, K. J. Ahn, Y. Kang, and K.-G. Lee, "Organic-inorganic FAPbBr₃ perovskite quantum dots as a quantum light source: Single-photon emission and blinking behaviors," *ACS Photonics* **5**(12), 4937–4943 (2018).
- ³¹G. Yuan, C. Ritchie, M. Ritter, S. Murphy, D. E. Gómez, and P. Mulvaney, "The degradation and blinking of single CsPbI₃ perovskite quantum dots," *J. Phys. Chem. C* **122**(25), 13407–13415 (2018).
- ³²S. Paul, G. Kishore, and A. Samanta, "Photoluminescence blinking of quantum confined CsPbBr₃ perovskite nanocrystals: Influence of size," *J. Phys. Chem. C* **127**(21), 10207–10214 (2023).
- ³³V. I. Klimov, A. A. Mikhailovsky, D. W. McBranch, C. A. Leatherdale, and M. G. Bawendi, "Quantization of multiparticle Auger rates in semiconductor quantum dots," *Science* **287**(5455), 1011–1013 (2000).
- ³⁴L. W. Wang, M. Califano, A. Zunger, and A. Franceschetti, "Pseudopotential theory of Auger processes in CdSe quantum dots," *Phys. Rev. Lett.* **91**(5), 056404 (2003).
- ³⁵I. Robel, R. Gresback, U. Kortshagen, R. D. Schaller, and V. I. Klimov, "Universal size-dependent trend in Auger recombination in direct-gap and indirect-gap semiconductor nanocrystals," *Phys. Rev. Lett.* **102**(17), 177404 (2009).
- ³⁶N. S. Makarov, S. Guo, O. Isaienko, W. Liu, I. Robel, and V. I. Klimov, "Spectral and dynamical properties of single excitons, biexcitons, and trions in cesium-lead-halide perovskite quantum dots," *Nano Lett.* **16**(4), 2349–2362 (2016).
- ³⁷Q. Li, Y. Yang, W. Que, and T. Lian, "Size- and morphology-dependent Auger recombination in CsPbBr₃ perovskite two-dimensional nanoplatelets and one-dimensional nanorods," *Nano Lett.* **19**(8), 5620–5627 (2019).
- ³⁸J. A. Castañeda, G. Nagamine, E. Yassitepe, L. G. Bonato, O. Voznyy, S. Hoogland, A. F. Nogueira, E. H. Sargent, C. H. B. Cruz, and L. A. Padilha, "Efficient biexciton interaction in perovskite quantum dots under weak and strong confinement," *ACS Nano* **10**(9), 8603–8609 (2016).
- ³⁹G. E. Eperon, E. Jedlicka, and D. S. Ginger, "Biexciton Auger recombination differs in hybrid and inorganic halide perovskite quantum dots," *J. Phys. Chem. Lett.* **9**(1), 104–109 (2018).
- ⁴⁰P. Huang, S. Sun, H. Lei, Y. Zhang, H. Qin, and H. Zhong, "Nonlocal interaction enhanced biexciton emission in large CsPbBr₃ nanocrystals," *eLight* **3**(1), 10 (2023).
- ⁴¹J. Liu and L. Coolen, "Auger effect in weakly confined nanocrystals," *Light Sci. Appl.* **12**(1), 179 (2023).
- ⁴²Y. Li, T. Ding, X. Luo, Z. Chen, X. Liu, X. Lu, and K. Wu, "Biexciton Auger recombination in mono-dispersed, quantum-confined CsPbBr₃ perovskite nanocrystals obeys universal volume-scaling," *Nano Res.* **12**(3), 619–623 (2019).
- ⁴³V. I. Klimov, J. A. McGuire, R. D. Schaller, and V. I. Rupasov, "Scaling of multiexciton lifetimes in semiconductor nanocrystals," *Phys. Rev. B* **77**(19), 195324 (2008).
- ⁴⁴B. Fisher, J. M. Caruge, Y. T. Chan, J. Halpert, and M. G. Bawendi, "Multiexciton fluorescence from semiconductor nanocrystals," *Chem. Phys.* **318**(1–2), 71–81 (2005).
- ⁴⁵H. Htoon, J. A. Hollingsworth, R. Dickerson, and V. I. Klimov, "Effect of zero- to one-dimensional transformation on multiparticle Auger recombination in semiconductor quantum rods," *Phys. Rev. Lett.* **91**(22), 227401 (2003).
- ⁴⁶F. R. Hu, H. C. Zhang, C. Sun, C. Y. Yin, B. H. Lv, C. F. Zhang, W. W. Yu, X. Y. Wang, Y. Zhang, and M. Xiao, "Superior optical properties of perovskite nanocrystals as single photon emitters," *ACS Nano* **9**(12), 12410–12416 (2015).
- ⁴⁷W. Guo, J. Tang, G. Zhang, B. Li, C. Yang, R. Chen, C. Qin, J. Hu, H. Zhong, L. Xiao, and S. Jia, "Photoluminescence blinking and biexciton Auger recombination in single colloidal quantum dots with sharp and smooth core/shell interfaces," *J. Phys. Chem. Lett.* **12**(1), 405–412 (2021).
- ⁴⁸X. Q. Hou, J. Kang, H. Y. Qin, X. W. Chen, J. L. Ma, J. H. Zhou, L. P. Chen, L. J. Wang, L. W. Wang, and X. G. Peng, "Engineering Auger recombination in colloidal quantum dots via dielectric screening," *Nat. Commun.* **10**(1), 1750 (2019).
- ⁴⁹R. Y. Meng, H. Y. Qin, Y. Niu, W. Fang, S. Yang, X. Lin, H. J. Cao, J. L. Ma, W. Z. Lin, L. M. Tong, and X. G. Peng, "Charging and discharging channels in photoluminescence intermittency of single colloidal CdSe/CdS core/shell quantum dot," *J. Phys. Chem. Lett.* **7**(24), 5176–5182 (2016).
- ⁵⁰P. P. Jha and P. Guyot-Sionnest, "Trion decay in colloidal quantum dots," *ACS Nano* **3**(4), 1011–1015 (2009).
- ⁵¹A. Swarnkar, A. R. Marshall, E. M. Sanehira, B. D. Chernomordik, D. T. Moore, J. A. Christians, T. Chakrabarti, and J. M. Luther, "Quantum dot-induced phase stabilization of α -CsPbI₃ perovskite for high-efficiency photovoltaics," *Science* **354**(6308), 92–95 (2016).
- ⁵²P. Spinicelli, S. Buil, X. Quélin, B. Mahler, B. Dubertret, and J. P. Hermier, "Bright and grey states in CdSe-CdS nanocrystals exhibiting strongly reduced blinking," *Phys. Rev. Lett.* **102**(13), 136801 (2009).
- ⁵³B. Li, G. F. Zhang, Z. Wang, Z. J. Li, R. Y. Chen, C. B. Qin, Y. Gao, L. T. Xiao, and S. T. Jia, "Suppressing the fluorescence blinking of single quantum dots encased in N-type semiconductor nanoparticles," *Sci. Rep.* **6**, 32662 (2016).
- ⁵⁴G. Nair, J. Zhao, and M. G. Bawendi, "Biexciton quantum yield of single semiconductor nanocrystals from photon statistics," *Nano Lett.* **11**(3), 1136–1140 (2011).
- ⁵⁵B. Li, Y. Gao, R. Wu, X. Miao, and G. Zhang, "Charge and energy transfer dynamics in single colloidal quantum dots/monolayer MoS₂ heterostructures," *Phys. Chem. Chem. Phys.* **25**(11), 8161–8167 (2023).

⁵⁶H. Igarashi, M. Yamauchi, and S. Masuo, "Correlation between single-photon emission and size of cesium lead bromide perovskite nanocrystals," *J. Phys. Chem. Lett.* **14**(9), 2441–2447 (2023).

⁵⁷M. Zhu, J. Zhou, Z. Hu, H. Qin, and X. Peng, "Effects of local dielectric environment on single-molecule spectroscopy of a CdSe/CdS core/shell quantum dot," *ACS Photonics* **5**(10), 4139–4146 (2018).

⁵⁸K. E. Shulenberger, T. S. Bischof, J. R. Caram, H. Utzat, I. Coropceanu, L. Nienhaus, and M. G. Bawendi, "Multiexciton lifetimes reveal triexciton emission pathway in CdSe nanocrystals," *Nano Lett.* **18**(8), 5153–5158 (2018).

⁵⁹K. F. Wu, J. Lim, and V. I. Klimov, "Superposition principle in Auger recombination of charged and neutral multicarrier states in semiconductor quantum dots," *ACS Nano* **11**(8), 8437–8447 (2017).